Article

Not peer-reviewed version

Thermostratigraphic and Heat Flow Assessment of the South Slave Region in the Northwest Territories, Canada

Mirah Rajaobelison * , Michaël Thibault , Félix-Antoine Comeau , Jasmin Raymond * , Emily J Smejkal , Viktor Terlaky

Posted Date: 9 May 2024

doi: 10.20944/preprints202405.0565.v1

Keywords: Hay River; geothermal energy; thermal conductivity; heat flow; Western Canadian Sedimentary Basin

Article

Thermostratigraphic and Heat Flow Assessment of the South Slave Region in the Northwest Territories, Canada

Mirah Rajaobelison [1,*], Michaël Thibault [1], Félix-Antoine Comeau [1], Jasmin Raymond [1,*], Emily J. Smejkal [2] and Viktor Terlaky [3,]

[1] Centre Eau Terre Environnement—Institut national de la recherche scientifique 490, rue de la Couronne. Québec (Québec) G1K 9A9, Canada; michael.thibault@inrs.ca (M.T.); felix-antoine.comeau@inrs.ca (F.-A.C.)
[2] Terrapin Geothermics Inc 750, 10707-100 Ave NW, Edmonton, AB, T5J 3M1, Canada Emily.J.Smejkal@outlook.com (E.J.S.)
[3] Northwest Territories Geological Survey 4601-B 52 Avenue, Yellowknife NT, X1A 2L9, Canada viktor_terlaky@gov.nt.ca (V.T.)
* Correspondence: miora_mirah.rajaobelison@inrs.ca (M.R.); jasmin.raymond@inrs.ca (J.R.)

Abstract: Despite the elevated heat flow known in the Western part of the South Slave Region (Northwest Territories, Canada), a continuous and equilibrium geothermal gradient was never measured in boreholes below the communities where geothermal energy could be developed. This paper aims to predict the geothermal gradient and assess the Earth's natural heat flow below the communities of Fort Providence, Kakisa, Hay River, and Enterprise. Temperatures from drill-stem test and bottom well logs were corrected for drilling disturbance and paleoclimates. Thermal conductivity and heat generation rate of the geological formations were determined from the literature and with new laboratory measurements. 1D models were developed to evaluate subsurface temperature through the sedimentary formations, based on a thermostratigraphic assessment. Results indicate a geothermal gradient varying from 44.1 ± 10.6 °C km^{-1} to 59.1 ± 14.9 °C km^{-1} and heat flow varying from 105.5 mW m^{-2} to 160.2 mW m^{-2} below the communities. These estimates are in agreement with the equilibrium geothermal gradients measured in the Cameron Hills, south of the four communities, and used to verify our predictions. Hay River appears to be the most promising community with the highest geothermal gradient estimated to be 59.1 ± 14.9 °C km^{-1}.

Keywords: Hay River; geothermal energy; thermal conductivity; heat flow; Western Canadian Sedimentary Basin

---

1. Introduction

Estimating the geothermal gradient and terrestrial heat flow are important steps in assessing the geothermal potential of a region. This is usually done through measurement of an equilibrium temperature profile [1,2]. The thermal conductivity of the geological materials underlying the region also needs to be measured. This kind of heat flow assessment is crucial for any geothermal development, but can be expensive, because it usually requires an exploration borehole specifically drilled for geothermal purposes [3]. In remote communities of the Canadian North that have populations of a few hundred to less than four-thousand people, drilling such boreholes is difficult to justify in the early exploration stage. However, geothermal gradient and heat flow can be predicted at the early exploration phase with 1D models that rely on a thermostratigraphic assessment and corrected downhole temperatures [1,4–6]. This approach can better inform decision-making regarding the exploitability of clean and reliable local geothermal heat for such remote communities.

The geothermal potential of the South Slave Region of the Northwest Territories (NWT) is studied with this perspective in mind, using a community approach to evaluate the thermal state and properties below—from North to South—Fort Providence, Kakisa, Hay River, and Enterprise (Figure 1). The most recent map of heat flow in Canada [7], updated from Grasby et al. [8], indicates heat

Preprints.org (www.preprints.org) | NOT PEER-REVIEWED | Posted: 9 May 2024 doi:10.20944/preprints202405.0565.v1

flow values in the South Slave region from 40 mW m^{-2} to 100 mW m^{-2}, which is the highest in the Western Canada Sedimentary Basin (WCSB). The work of EBA Engineering Consultants Ltd. [9] has shown very high geothermal favourability and potential in NWT to the west of Great Slave Lake (Figure 1b). To support geothermal research in the South Slave region, Petrel Robertson Consulting Ltd. [10] identified 109 oil and gas wells between 48 m and 1500 m depth that were cored and have publicly available geoscience data that could be further investigated. A total of 68 of these wells have bottom-hole temperature (BHT) and drill-stem test (DSTs) records from publicly available historic well files. Individual Well History Files from the archives of the Office of the Regulator of Oil and Gas Operations [11] was also consulted to supplement the temperature data. Oil and gas wells were recently abandoned in the Cameron Hills located about 100 km to the southwest of the studied communities. Smejkal et al. [12] took the opportunity to access these wells during abandonment activities, and measured an equilibrium temperature profile in six deep wells and evaluated the geothermal gradient.

Terrestrial heat flow estimates from analysis of BHT data exist for several sedimentary basins around the world, including Brazil [13], Western Canada [14], Eastern Canada [15] and the St. Lawrence Lowlands in Québec [4]. Drill-stem test temperature based on flowing oil or water from the producing formation is generally a reliable source of data for the calibration of basin system models [16], but are not as common as BHT measurements. On the other hand, BHTs from well log headers are available for most wells, but are biased and usually lower than the equilibrium formation temperature [17]. Hence, correction for drilling disturbances is necessary and ideally requires multiple BHT measurements at successive times in order to find the equilibrium temperature. The analytical Horner technique is a commonly used method to correct multiple BHT measurements [18]. Criteria for reliable Horner corrected BHTs include a minimum of three logging runs that record time and temperature for each run, and deviation from the least squares regression line that is less than the measurement uncertainty [i.e., ± 1-3 °C; [16]]. Other correction schemes that do not use mud circulation time and are typically empirical include the Förster Correction [19], the Harrison Correction [6], subsequently redefined by Blackwell et al. [20], and Blackwell [21], and the Kehle Correction [22]. These correction schemes were used for correcting BHTs in the Denver Basin of Colorado and in Nebraska [23]. However, these empirical corrections are not always appropriate to use in all basins since the difference in lithologies and thermal histories may affect the correction [23,24]. Heat flow estimates, especially based on temperature measurements at shallow depth, additionally require corrections for paleoclimate effects [25]. These effects must be taken into account in the South Slave Region, which was covered by the Laurentide Ice Sheet during the last glaciation (Late Wisconsinan) ~25–10 ka [26,27], resulting in a decrease in subsurface temperature through thermal diffusion.

In this study, our objective is to reevaluate the heat flow and predict the geothermal gradient with 1D models in the four main South Slave communities that are at an early geothermal exploration stage. This paper provides a widely applicable workflow of local geological assessment that can be used to plan the drilling of exploration boreholes, helping to move to the next step of geothermal development in small and remote communities. Relying on available data, we use a community approach rather than a regional assessment to predict the thermal state and properties below population centers where geothermal energy can be used. We believe it is the most appropriate method for such a remote region where the population is sparse and geothermal energy exportation is hindered by the lack of infrastructure. Our assessment comprises analysis of publicly available data from oil and gas wells nearby the four communities and include BHT and DST data combined with vertical thermal conductivity profiles deduced from core analysis and corresponding lithological profiles beneath the communities. A 1D thermostratigraphic model for each community is developed and is verified with equilibrium temperature data obtained from Cameron Hills.

2. Geological Setting

The portion of the South Slave Region of interest is delineated by the coordinates 60°N, 111°W in the SE to 62°N, 120°W in the NWT (Figure 1a). This area is located in the Interior Platform, which

 doi:10.20944/preprints202405.0565.v1

constitutes the northern extension of the WCSB, and is bounded by the Canadian Shield to the East and the Mackenzie Mountains to the West [28] and references therein. The Interior Platform is divided into two domains or exploration areas, including the Great Bear Plain and Great Slave Plain. The area of interest for this study is in the Great Slave Plain [Figure 1a; [29]].

The geology of the Great Slave Plain comprises Precambrian metasedimentary and crystalline basement rocks overlain by Paleozoic and Mesozoic sedimentary rocks, and Quaternary overburden with variable thickness. The dominant lithologies making up the Paleozoic and Mesozoic sedimentary strata are shale, limestone, marine dolostone, anhydrite and sandstone. Devonian rocks make up the bulk of the sedimentary strata underlying the communities, illustrated by the cross-sections in Figure 2b; for a detailed review and description of the Devonian stratigraphy see Meijer Drees [30], Moore [31], Morrow et al. [32], Mossop et al. [33], among others.

According to the works of Gal et al. [28], the local stratigraphy comprises a relatively thin (500 m to 700 m) Paleozoic and Mesozoic sedimentary cover overlying the Precambrian basement (Figure 2b). This is confirmed by the Phanerozoic isopach map of the WCSB [34].

Smith et al. [35] provides the most recent drift isopach model including the thickness of Quaternary glacial sediment. The drift cover in the South Slave is up to 150 m thick, but has considerable variation; the majority of the cover is less than 10 m thick, and sporadically sedimentary rocks outcrop in the area. However, the drift thickness is locally up to 400 m thick at Cameron Hills.

Deep-seated faults and horst and graben block faulting of basement rocks stretching to the Cameron Hills area resulted from an extensional tectonic regime in the late Precambrian. This extensional tectonic regime was reactivated and influenced the Phanerozoic sediment cover. The major faults and fault zones that affected the area have a Northeast trend [Figure 2]; [28,36].

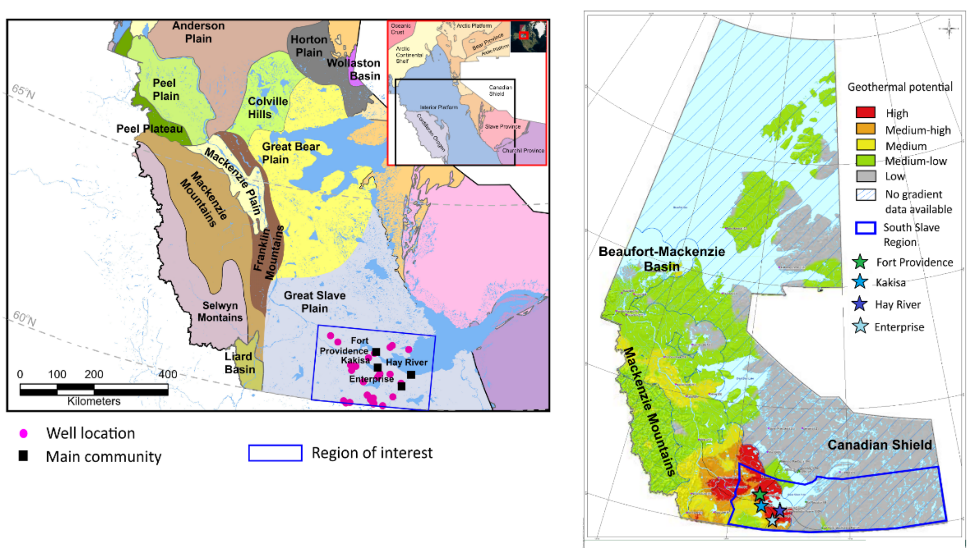

(a) (b)

Figure 1. a) Geological provinces and exploration areas base map with the location of the study area outlined in blue [modified from 36]. Pink dots indicate the location of sampled wells. The well locations are from the map of Petrel Robertson Consulting Ltd. [10]. b) Geothermal feasibility map of the Northwest Territories modified from EBA Engineering Consultants Ltd. [9].

Preprints.org (www.preprints.org) | NOT PEER-REVIEWED | Posted: 9 May 2024 doi:10.20944/preprints202405.0565.v1

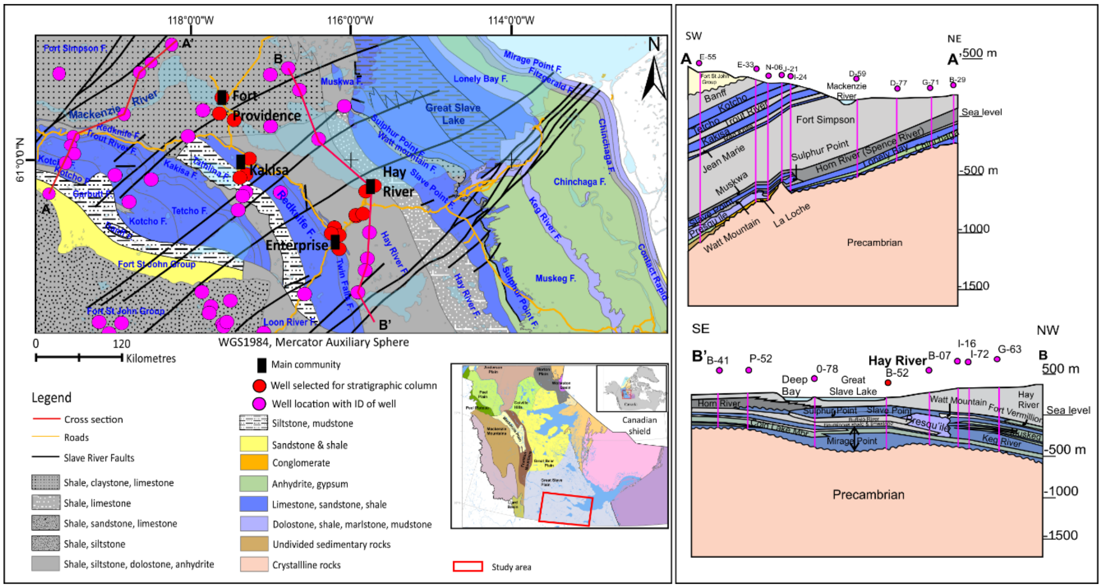

(a) (b)

Figure 2. a) Geological map of the study area [modified from [37]]. The well locations were taken from the Geothermal Database Compilation Devonian Cores Map from Petrel Robertson Consulting Ltd. [10] and Gal et al. [28]. b) Cross sections showing stratigraphic and chronological relationships of the dominant lithologies and their corresponding formations in the Great Slave Plain (modified from Gal et al. [28]).

3. Input Data

The data set consists of information from 75 of the 116 wells in the area of interest (Figure 3), which were made available from the Petrel Robertson Consulting Ltd. [10] Excel file and from the Individual Well History Files from OROGO [11]. The wells with DST and/or BHT data were also chosen to be as close as possible to the four main communities. The equilibrium temperature profiles recorded in 2023 from six wells (A-73, E-07, I-10, I-74, L-44, M-49) in the Cameron Hills region are located close enough to the study area (Figure 3) to be used for verification purposes.

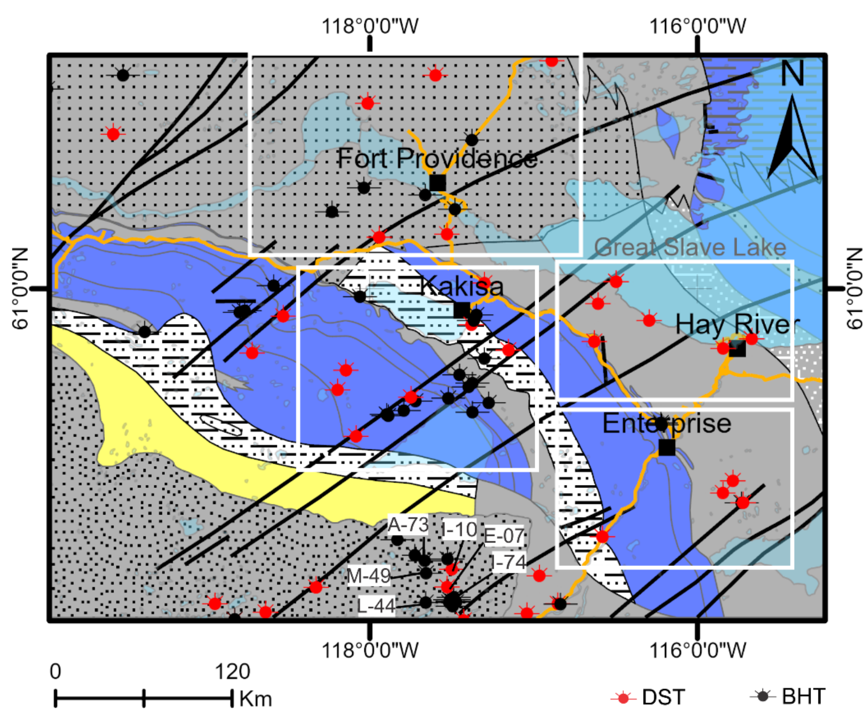

Preprints.org (www.preprints.org) | NOT PEER-REVIEWED | Posted: 9 May 2024 doi:10.20944/preprints202405.0565.v1

Figure 3. Location of the 75 wells with measured DST and BHT. The white boxes delineate the wells selected for each community. The wells with ID are those in the Cameron Hills region that have equilibrium temperature data. The geological base map is modified from the Northwest Territories Geological Survey [37] and has the same legend as Figure 2.

3.1. Temperature Data

3.1.1. South Slave Region

A total of 33 of the 75 wells have a DST temperature record. BHTs were measured in 42 wells at depths from 504 m to 1657 m (Table 1).

Table 1. Temperature data from wells.

Data type	Number of wells	Depth *TVD* [m]	Temperature [°C]	Source
DST	20 5	≥ 600-1846 < 600	19-63	Petrel Robertson Consulting Ltd. [10]
	4 3	≥ 600-941 < 600	17-42	OROGO [11]
BHT	36 5	≥ 600-1657 < 600	26-76	Petrel Robertson Consulting Ltd. [10]
	1 1	≥ 600 < 600	27	OROGO [11]
No data	41			Petrel Robertson Consulting Ltd. [10]
Total	116	49 -1949	17-76	

Set as the upper boundary condition in our model, the average annual undisturbed ground temperature T_s (°C) was obtained by converting the air -temperature to ground-temperature using an empirical relationship. The following equation developed by Ouzzane et al. [39] was used for this purpose:

$$T_s = 17.898 + 0.951 T_{amb}, \quad (1)$$

where T_s (K) is the undisturbed ground surface temperature and T_{amb} (K) is the annual ambient temperature, which is -2.5 °C for the region. This mean annual air temperature was obtained from the Hay River-A weather station [40]. T_s was consequently estimated to be 2.1 °C.

3.1.2. Cameron Hills

The equilibrium temperature data from wells in the Cameron Hills were chosen because the stratigraphy, which was confirmed with gamma ray (*GR*) log [12], shares similarities with that of the South Slave communities. The stratigraphic formations and corresponding lithology were taken from the Table of Formation tops established by Gal et al. [28] and Rocheleau et al. [37]. In the Cameron Hills, T_s was evaluated from the temperatures measured at the top of the Cretaceous basal sandstone (CB SS unit) marking the base of the clastic Cretaceous section underlying the Devonian carbonates, since continuous temperature profiles were available at this geological formation at depth around 500 m [12].

3.2. Thermal Conductivity and Heat Generation Rate

Preprints.org (www.preprints.org) | NOT PEER-REVIEWED | Posted: 9 May 2024 doi:10.20944/preprints202405.0565.v1

3.2.1. South Slave Region

Thermostratigraphic logs were initially created for the four South Slave communities combining the stratigraphic column that approximates the thickness of the main stratigraphic formations, with the corresponding subsurface thermal conductivity [41] (Table 2; Figure 4). These local stratigraphic columns gave an extended and refined geological model under each community, showing that the Precambrian basement lies at a shallow depth of 500 m to 700 m. Shale is the dominant lithology over the total thickness of sedimentary rocks (~600 m) in Fort Providence, Kakisa, and Enterprise. Carbonate rocks is 600 m thick and the shale cover is approximately 100 m thick at Hay River location. Near-surface, quaternary sediments overlying the Paleozoic rocks are less than 10 m thick, and are omitted, because the sedimentary deposits do not contribute enough to heat transfer when calculating the geothermal gradient and heat flow from deep rocks (e.g., Beardsmore et al. [42]; Jaupart et al.[43]). Laboratory assessment of the thermal conductivity was completed on 84 split core samples from 33 wells that cover seven geological formations. Measurements were carried out at the Laboratoire ouvert de géothermie at the Institut national de la recherche scientifique (INRS) in Canada using an optical scanning instrument following the methodology of Popov et al.[44]. For some formations there was no core available for measurement; the thermal conductivity value for these were taken from literature [8] and references therein , [45,46] and references therein, [47–51].

The average heat generation rate A (W m^{-3}) for lithological formations below the South Slave Communities was evaluated using the empirical equation of Bücker et al. [52] which relates heat generation to the concentration of uranium *[U]*, thorium *[Th]* and potassium *[K].* The concentration of these radiogenic elements was determined by means of inductively coupled plasma analyses at INRS geochemical Laboratory [41]. Although laboratory measurements were made on available core material, this was insufficient to cover all geological formations. Consequently, heat generation rates were assumed by analogy with lithologically similar formations where it was evaluated. Additionally, literature values of heat generation rate [53,54] and references therein] were assigned to the sedimentary rock type for formations with no core.

Table 2. Thermal conductivity and heat generation rate for South Slave Communities.

Formation	**Lithology**	***n***	**Heat Production** A	**Thermal conductivity**	
				Lithology Mean	**Formation Mean**
			[W m^{-3}]	**λ [W m^{-1} K^{-1}]**	
Alluvium	Sand		1.7×10^{-6}	1.4	1.4
Twin Falls	Limestone		0.19×10^{-6}	2.5	2.5
	Shale		0.53×10^{-6}	2.1	
Hay River	Shale		0.53×10^{-6}	2.1	2.1
	Limestone		0.19×10^{-6}	2.5	
Hay River (Escarpment)	Shale		0.53×10^{-6}	2.1	2.1
	Limestone		0.19×10^{-6}	2.5	
Hay River (Waterways)	Shale		0.53×10^{-6}	2.1	2.2
	Limestone		0.19×10^{-6}	2.5	
Slave Point	Limestone	25	0.25×10^{-6}	2.9	2.9
	Dolostone	4	0.13×10^{-6}	4.6	
Horn River	Shale		0.53×10^{-6}	2.1	2.1
	Limestone		0.19×10^{-6}	2.5	
Watt Mountain	Shale		0.53×10^{-6}	2.1	2.2
	Limestone	8	0.11×10^{-6}	3.1	
	Sandstone		1.70×10^{-6}	3.4	
Sulphur Point	Dolostone	7	0.11×10^{-6}	4.4	3.5
	Limestone	13	0.18×10^{-6}	3.4	
	Shale		0.53×10^{-6}	2.1	

 doi:10.20944/preprints202405.0565.v1

	Limestone		0.19×10^{-6}	2.5	
Muskeg	Dolostone	6	0.09×10^{-6}	5.0	4.4
	Anhydrite	1	0.02×10^{-6}	5.6	
Klua	Shale		0.53×10^{-6}	2.1	2.1
	Limestone		0.19×10^{-6}	2.5	
Keg River	Dolostone	8	0.13×10^{-6}	4.9	3
	Limestone		0.19×10^{-6}		
Lonely Bay	Dolostone		0.11×10^{-6}	3.8	3
	Limestone		0.19×10^{-6}	2.5	
Chinchaga	Anhydrite	2	0.08×10^{-6}	4.8	3.6
	Dolostone	4	0.11×10^{-6}	4.2	
	Shale		0.53×10^{-6}	2.1	
	Limestone		0.19×10^{-6}	2.5	

n: number of samples

Formation	**Lithology**	***n***	**Heat Production *A***	**Thermal conductivity**	
				Lithology Mean	**Formation Mean**
			[W m^{-3}]	**λ [W m^{-1} K^{-1}]**	
Chinchaga (Ebutt Member)	Shale		0.53×10^{-6}	2.1	3.6
	Limestone		0.19×10^{-6}	2.5	
	Dolostone		0.11×10^{-6}	3.8	
	Anhydrite		0.08×10^{-6}	4.3	
Headless	Limestone		0.19×10^{-6}	2.5	2.3
	Shale		0.53×10^{-6}	2.1	
	Dolostone		0.11×10^{-6}	3.8	
Mirage Point	Shale		0.53×10^{-6}	2.1	2.6
	Dolostone		0.11×10^{-6}	3.8	
	Halite		0.08×10^{-6}	5.0	
	Anhydrite		0.08×10^{-6}	4.3	
Mirage Point (Ernestina Lake)	Dolostone		0.11×10^{-6}	3.8	3.3
	Anhydrite		0.08×10^{-6}	4.3	
	Shale		0.53×10^{-6}	2.1	
La Loche	Sandstone		1.70×10^{-6}	3.4	3.4
	Shale		0.53×10^{-6}	2.1	
La Loche (Red Beds)	Sandstone		1.70×10^{-6}	3.4	3.4
La Loche (Basal Clastics)	Sandstone		1.70×10^{-6}	3.4	3.4
	Total	80			

n: number of samples

Preprints.org (www.preprints.org) | NOT PEER-REVIEWED | Posted: 9 May 2024 doi:10.20944/preprints202405.0565.v1

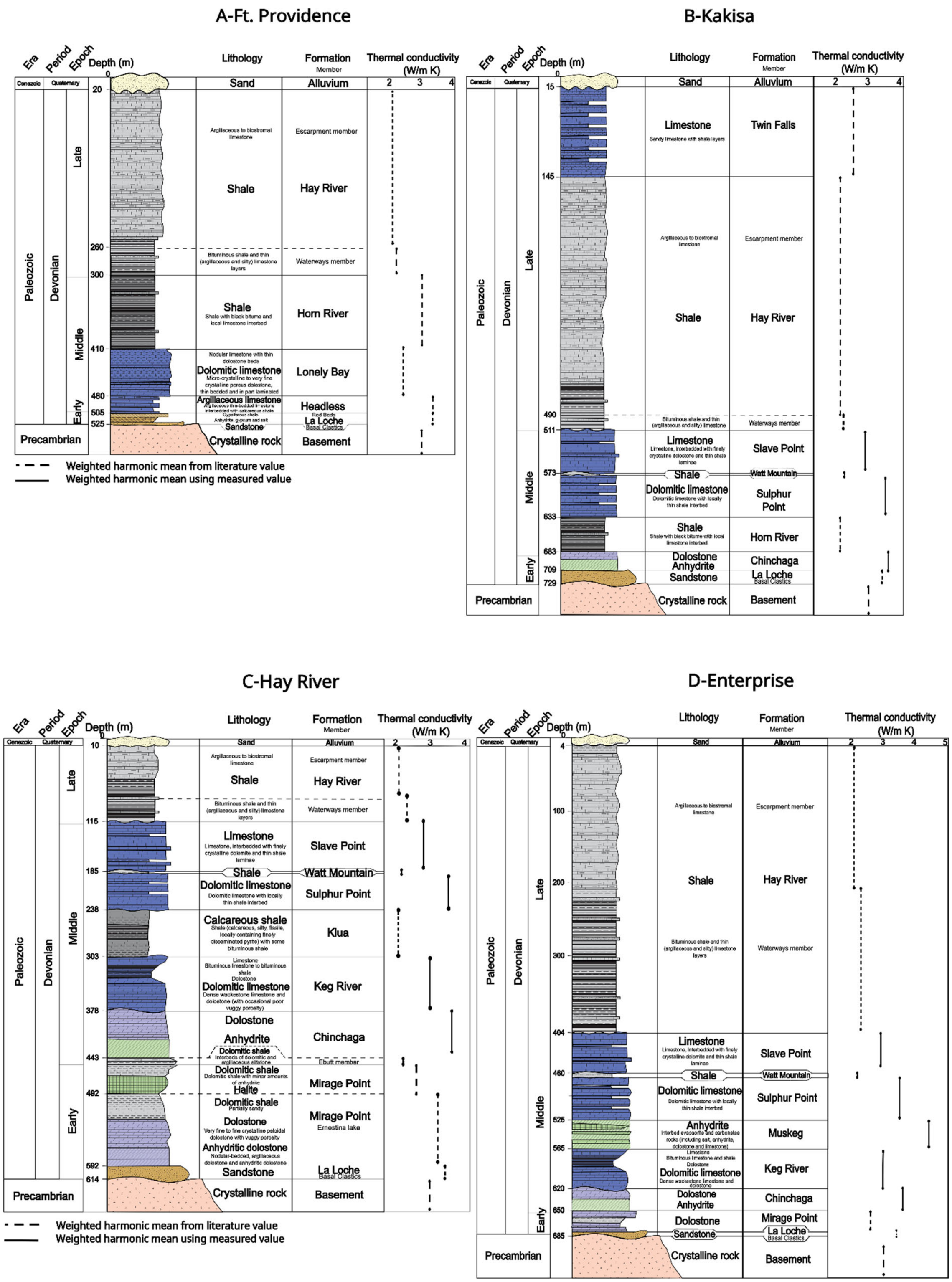

Figure 4. Thermostratigraphic log at the location of the four South Slave communities reproduced from Rajaobelison et al. [40].

3.2.2. Cameron Hills

Core materials were not available for the Cameron Hills wells and geological formations encountered here. Thermal conductivity here was determined with analogy to thermal conductivity

 doi:10.20944/preprints202405.0565.v1

measurements made on core samples for the South Slave Formations from Rajaobelison et al. [41] (Table 2; Figure 4).

The internal heat generation rate for rocks A (W m^{-3}) intersected by Cameron Hills wells was calculated from the gamma ray log (GR; American Petroleum Institute units) according to equation [2] from Burrus et al. [55]:

$$A = 0.0145 \times (GR - 5) \quad (2)$$

The average heat production rate for each formation was calculated from the arithmetic average GR measured between the top and base of each corresponding formation (Table 3).

Table 3. Thermal conductivity and heat generation rate of Cameron Hills geological formations.

Well short name	Geological formations	Top	Lithology	λ	GR	A
		[m]		[W m^{-1} K^{-1}]	[API]	[W m^{-3}]
A-73	Wabamun	443	Dolomitic limestone	3.5	49.0	0.64×10-6
	TwinFalls	809	Limestone	2.5	34.6	0.43×10-6
	Muskwa	1022	Organic-rich shale	2.1	23.5	0.27×10-6
	Waterways	1283	bituminous shale	2.1	11.2	0.09×10-6
E-07	CB SS	461.4	Sandstone	3.4	30.7	0.37×10-6
	Wabamun	471.9	Dolomitic limestone	3.5	32.5	0.40×10-6
	Twin Falls	760	Limestone	2.5	31.8	0.39×10-6
	Hay River	912.5	Shale	2.2	60.6	0.81×10-6
I-10	CBS SS	575.1	Sandstone	3.4	43.3	0.56×10-6
	Wabanum	590.3	Dolomitic limestone	3.5	17.9	0.19×10-6
	Trout River	622	Shale	2.1	15.1	0.15×10-6
	Kakisa	627.9	Limestone	3.0	16.7	0.17×10-6
	RedKnife	665.8	Shale	2.1	57.8	0.77×10-6
	Tathlina	715	Shale	2.1	35.1	0.44×10-6
	Twin Falls	868.3	Limestone	2.5	27.6	0.33×10-6
	Hay River	999.5	Shale	2.1	50.5	0.66×10-6
I-74	BS SS	539.7	Sandstone	3.4	31.5	0.38×10-6
	Wabamun	554.6	Dolomitic limestone	3.5	17.0	0.17×10-6
	Ft.Simpson	717.6	Limestone	3.0	39.2	0.50×10-6
	Twin Falls	829.1	Limestone	2.5	20.4	0.22×10-6
	Hay River	898.8	Shale	2.1	44.5	0.57×10-6
L-44	CB SS	516.8	Sandstone	3.4	30.6	0.37×10-6
	Wabamun	528.2	Dolomitic limestone	3.5	40.6	0.52×10-6
	Twin Falls	855	Limestone	2.2	70.8	0.95×10-6
	Hay River	1022	Shale	2.1	68.3	0.92×10-6
	Beaverhill Lake	1305.2	anhydrite and Limestone	4.3	49.0	0.64×10-6
M-49	CBS SS	471.6	Sandstone	3.4	33.1	0.41×10-6
	Wabanum	478.1	Dolomitic limestone	3.5	33.1	0.41×10-6
	Ft. Simpson	696.5	Shale	3.0	20.2	0.22×10-6
	Twin Falls	812.8	Limestone	2.5	46.5	0.60×10-6
	Hay River	961.9	Shale	2.1	32.2	0.39×10-6
	Beaverhill Lake	1252.6	Anhydrite and Carbonates	4.3	60.5	0.80×10-6
	Slave Point	1301.9	Limestone	2.9	56.6	0.75×10-6

4. Methods

Preprints.org (www.preprints.org) | NOT PEER-REVIEWED | Posted: 9 May 2024 doi:10.20944/preprints202405.0565.v1

Input temperature data were corrected for drilling disturbance and paleoclimates. Then, the geothermal gradient was calculated at the location of each community and for the Cameron Hill wells. The equilibrium temperature profile measured at the Cameron Hills was reproduced to verify if the thermal conductivity for each geological formation was adequately assigned. After the verification, the surface heat flow was calculated for the four communities and the 1D temperature profile below the four South Slave communities was predicted without paleoclimate correction using analytical calculations and assuming one dimensional conductive heat transfer with an internal heat generation in steady state.

4.1. Drilling Disturbance Correction for BHTs

Of the 75 wells, only 42 had one or two BHTs from wireline logs and mud circulation time was not provided. This is insufficient to meet the criteria for Horner correction [16]. Empirical corrections were therefore applied to the BHTs following the work of Crowell, Ochsner et al. [23]. The Harrison equation [6], the Kehle equation [56], the Förster (a) equation [19] and the Förster (b) equation [57] were considered for corrections, because the lithology of the South Slave Region is similar to that of the basins in which these corrections were developed [19,23]:

$$T_{cf}\ (°C) = -16.51 + 0.018 \times TVD - 2.345 \times 10^{-6} \times TVD^2, \quad (3)$$

$$T_{cf}\ (°F) = -8.819 \times 10^{-12} \times TVD - 2.143 \times 10^{-8} \times TVD^2 + 4.375 \times 10^{-3} \times TVD - 1.018, \quad (4)$$

$$T_{cf}\ (°C) = 0.012 \times TVD - 3.68, \quad (5)$$

$$T_{cf}\ (°C) = 0.017 \times TVD - 6.58. \quad (6)$$

where T_{cf} (°C/°F) is the temperature coefficient correction added to the BHT and TVD (m/in feet for Kehle equation) is the true vertical depth at which the BHT was measured.

Then, the best correction method was chosen based on the best fit to the geothermal gradient calculated from DST temperatures [19]. The corrections were established for depths from 600 m to 3 km, thus temperatures recorded in South Salve wells at depths shallower than 600 m were not corrected. However, uncorrected temperatures at depth between 300 m and 600 m was retained when the gradient was evaluated at the scale of the community due to limited data availability and for more accuracy.

4.2. Paleoclimate Correction

Quaternary glaciation periods are expected to have disturbed the subsurface temperature in the South Slave Region, as paleoclimate perturbations were recorded in the temperature signal of deep boreholes over more than 3 km depth in other nearby regions of Canada [58–60]. BHT and DST temperatures are assumed to have recorded significant Holocene and Pleistocene climatic perturbations. Based on the ground temperature history and the method of Birch [61], the temperature during the Pleistocene glacial cycles in Canada has been considered to be 5 °C colder during the glaciations [1,62]. At the beginning and end of each glaciation, this is the magnitude of temperature change or the temperature step (T_i) that was assumed for the ground surface below the ice sheets [1; Figure 5].

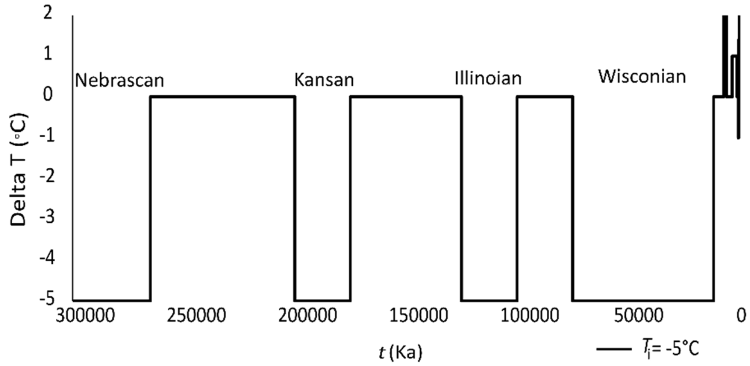

Figure 5. Timeline of Pleistocene and Holocene climate events according to a relative change of temperature of 5 °C modified from Bédard et al. [4].

The temperature at any depth corrected for paleoclimate effects is (e.g., Jessop (1990):

$$T_c = T_m + \sum\nolimits_i (T_i) \left[erf\left(\frac{z}{2\sqrt{\alpha\, t_1}}\right) - erf\left(\frac{z}{2\sqrt{\alpha\, t_2}}\right)\right] \quad (7)$$

where T_c (°C) is the temperature corrected for paleoclimate, T_m (°C) is the temperature measured at depth, T_i (°C) is the temperature step between glaciations, erf is the error function, α ($m^2\ s^{-1}$) is the rock thermal diffusivity (estimated to be ~1.44×10^{-6} considering the laboratory and thermostratigraphic assessments), t_1 (s) is the end of the ice age, t_2 (s) is the beginning of the ice age and z (m) is the depth of the temperature measurement.

4.3. Geothermal Gradient Calculation

Below each community, the average geothermal gradient g (°C m^{-1}) was calculated from the corrected temperature data of the nearest wells (Figure 3) using:

$$g = \frac{\Delta T}{\Delta z} = \frac{T_c - T_s}{\Delta TVD} \quad (8)$$

where ΔT (°C) is the difference between the corrected and the undisturbed ground temperature (T_s = 2.1 °C) divided by Δz (m), the true vertical depth difference. Depending on the purpose of the calculation, the corrected temperature can be BHT corrected for the drilling disturbance and paleoclimates when required or DST corrected for paleoclimates when required.

The geothermal gradient for Cameron Hills wells was determined from the slope calculation method using the temperature regression line of the measured profile. The average geothermal gradient g is the reverse of the slope.

4.4. Verification with Temperature Profiles from Cameron Hills

We used the equilibrium temperature profiles collect from the six wells in Cameron Hills to verify our thermostratigraphic model (Table 3 and Figure 4). This verified approached is then used to evaluate the heat flow (Q_0, W m^{-2}) and to predict temperature below the four South Slave communities where there are no equilibrium temperature profiles available. The heat flow at Cameron Hills was first calculated considering the equilibrium temperature at the bottom of the well. Then, temperature profiles recorded at the six Cameron Hills wells were recalculated according to the thermostratigraphic assessment made in South Slave communities. This temperature-depth model is to verify if the selected thermal properties for the geological formations are appropriate for the computed temperature to reproduce the observed temperature. The measured equilibrium temperature at the Cameron Hills wells are perturbed by paleoclimate effects. Therefore, no paleoclimate correction was made here to predict the ground temperature.

4.4.1. Heat Flow Evaluation for Cameron Hills

Equation (9) [1,41,42,45] allowed to calculate the surface heat flow Q_0 for Cameron Hill wells:

$$Q_0 = \lambda g + A\frac{z}{2} \tag{9}$$

where the thermal conductivity λ (W m^{-1} K^{-1}) is the weighted harmonic mean calculated from the lithological units, A (W m^{-3}) is the weighted arithmetic average heat generation in the sedimentary rock cover, z (m) is the thickness between the ground surface and measured temperature at both ends of the temperature profile and g (°C m^{-1}) is the geothermal gradient identified previously.

4.4.2. Temperature-Depth Models for Cameron Hills

The 1D calculation was made considering conductive heat transfer in steady-state conditions following [1,63,64]:

$$T_z = T_s + \frac{Q_0\, z}{\lambda} - A\frac{z^2}{2\lambda} \tag{10}$$

where T_z is the temperature at the depth z (m) in the sedimentary rock formations and Q_0 (W m^{-2}) was determined in the previous step, used as boundary conditions.

4.5. Prediction of Temperature Profiles for South Slave Communities

After verifying that our thermal conductivity assessment could accurately evaluate the temperature at depth for the Cameron Hills, the same approach was used to predict the temperature below the South Slave communities where no equilibrium temperature profile exists.

4.5.1. Heat Flow Evaluation for South Slave Communities

The surface heat flow Q_0 at the location of each community was now calculated using Equation (9). The stratigraphic column thickness z (m) was calculated from the surface to the top of the basement.

4.5.2. Temperature-Depth Model

1D temperature profiles below the four South Slave communities were calculated using Equation (10) and thermal conductivity validated with consideration for data from the Cameron Hills wells. The temperature profiles predicted in the sedimentary rock cover overlying the crystalline basement assumes steady state conductive heat transfer and considers internal heat generation at the location of the communities. The undisturbed ground temperature (T_s = 2.1 °C) and the surface heat flow Q_0 are the boundary conditions.

The calculation of the ground temperature is to reflect temperature that can be measured in sedimentary rocks below the South Slave communities such that the paleoclimate correction was not considered at this step. In this way, predicted temperature is perturbed by paleoclimates as expected when taking measurements less than 1 km deep.

5. Results

5.1. Corrected BHTs

Six of the 42 BHTs were not corrected because the temperature was recorded at depth less than 600 m. The Förster (a) correction revealed corrected BHTs closer to DST temperatures and a smaller standard deviation when compared to other correction methods (Figure 6). The correction factor T_{cf} (°C) obtained with Förster (a) method varied from 3.8 °C to 16.2 °C, resulting in corrected BHTs from 30.6 °C to 89.9 °C from 625.8 m to 1657 m depth.

 doi:10.20944/preprints202405.0565.v1

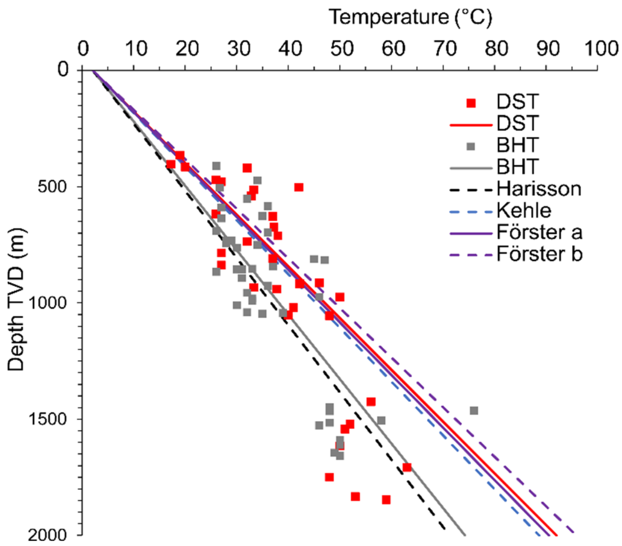

Figure 6. Uncorrected BHTs for the South Slave Region showing linear regression for corrected BHT compared to DST temperature and its trendline.

Due to the depth for which the correction method is developed, only one BHTs out of four in Ft. Providence and two out of the three in Enterprise could be corrected for the drilling disturbances (Table 4). Nevertheless, the non-corrected BHTs above minimum correction depth were kept to calculate the average geothermal gradient since measurements are relatively shallow and drilling disturbances expected to be less important. Only DST temperatures were available for Hay River.

Table 4. Temperature corrected for paleoclimates in each community.

		DST (*n*=5)	**Paleoclimate T_i=-5°C**	**BHT (*n*=4)**	**Förster (b)**	**Paleoclimate T_i=-5°C**
Fort-Providence	Min	20.0	21.4	26.7	41.3	43.1
	Max	37.0	38.8	36	41.3	43.1
		DST (*n*=7)	**Paleoclimate T_i=-5°C**	**BHT (*n*=14)**	**Khele**	**Paleoclimate T_i=-5°C**
Kakisa	Min	28.0	30.0	28.0	33.2	35.2
	Max	42.2	44.3	45.0	50.7	52.8
		DST (*n*=5)	**Paleoclimate T_i=-5°C**	**BHT (*n*=0)**		
Hay River	Min	19.0	20.3			
	Max	42.0	43.6			
		DST (*n*=2)	**Paleoclimate T_i=-5°C**	**BHT (*n*=3)**	**Harisson**	**Paleoclimate T_i=-5°C**
Enterprise	Min	17.2	18.6	27.0	23.6	25.5
	Max	56.0	58.5	34.0	21.2	22.9

n= number of temperature measurements

The most accurate correction method when analyzing each community individually is Förster (b) in Ft. Providence and Khele in Kakisa. Harisson method provided a better correlation with DST temperatures in Enterprise (Figure 7). It should be noted that the Harisson correction lowers the corrected temperature when the depth is less than 1000 m. The corresponding corrected temperature range is given in the Table 4.

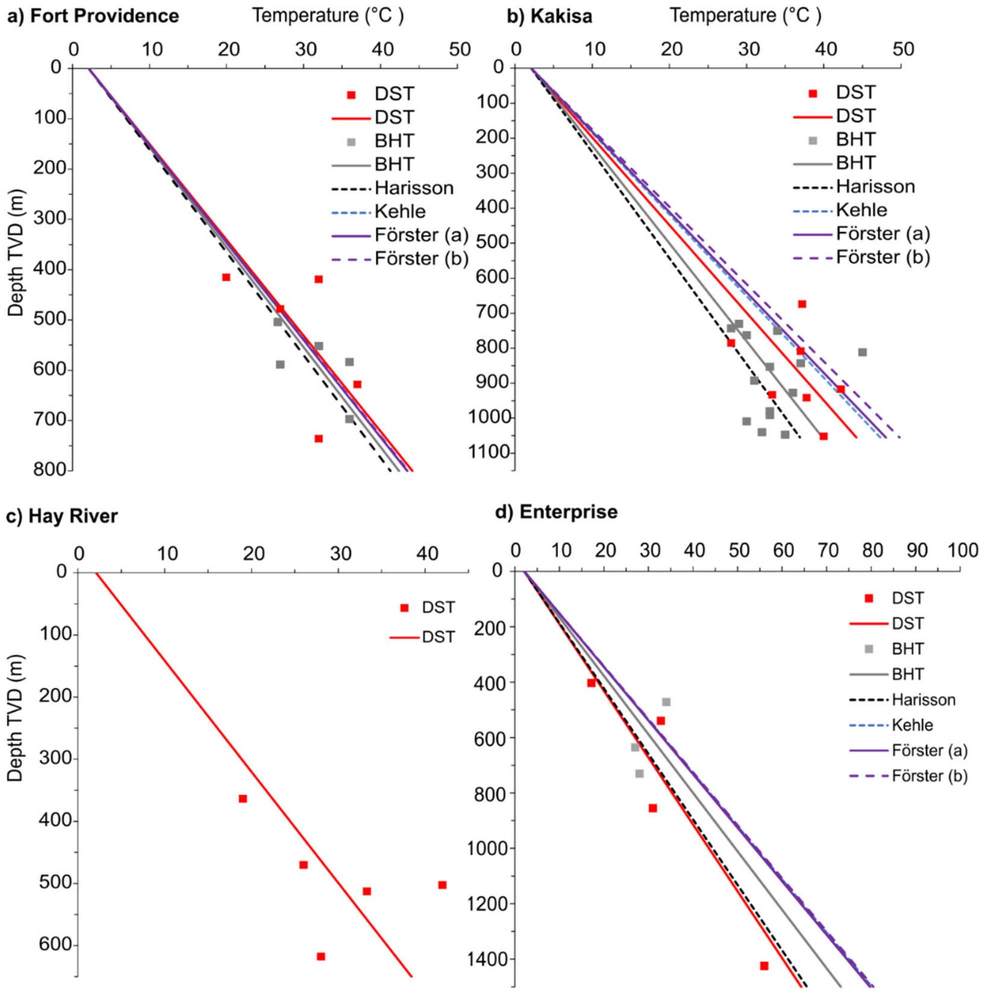

Figure 7. Uncorrected BHTs with the regression lines from corrected BHTs compared to DSTs temperature trendline for each community of the South Slave Region.

5.2. Paleoclimate Correction

The temperature correction varies between 1.1 °C and 2.5 °C from 364 m to 1846 m depth (Figure 8). The temperature range at each community are presented in Table 4.

Preprints.org (www.preprints.org) | NOT PEER-REVIEWED | Posted: 9 May 2024 doi:10.20944/preprints202405.0565.v1

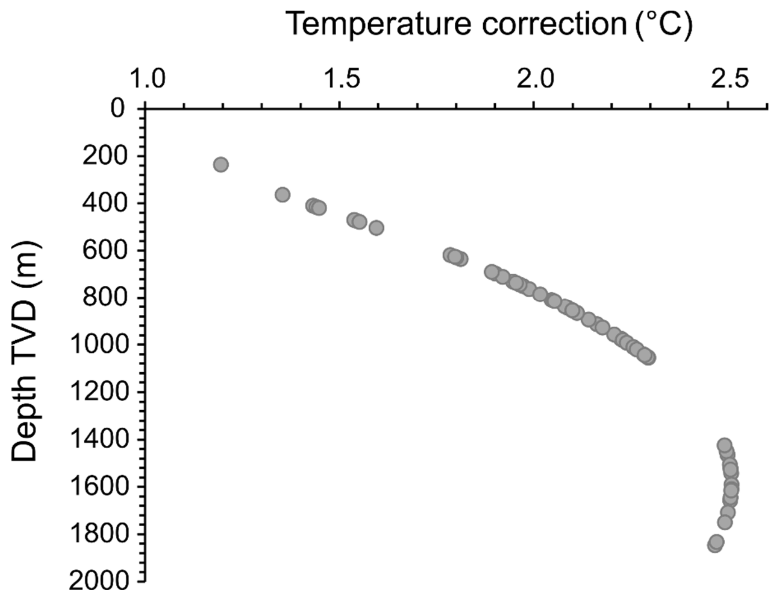

Figure 8. Paleoclimate temperature correction calculated as a funcion of depth at which DST and BHT were measured in the South Slave Region.

5.3. Geothermal Gradient

The geothermal gradients calculated from the BHTs recorded in 42 wells are from 27.6 °C km^{-1} to 55.1 °C km^{-1} with a mean of 36.1 ± 7.7 °C km^{-1}. After the drilling correction, the range of geothermal gradient is from 35.4 °C/km to 62.6 °C km^{-1}with an average of 44.3± 7.2 °C km^{-1}. The paleoclimate correction on DST temperatures and corrected BHTs revealed an average geothermal gradient of 45.6 ± 12.8 °C km^{-1}and 46.4 ± 7.5 °C km^{-1}, respectively (Table 5).

Table 5. Geothermal gradient (°C km^{-1}) in the South Slave Region.

	DST (*n*=33)	Paleoclimate T_i=-5°C	BHT (*n*=42)	Förster (a)	Paleoclimate T_i=-5°C
Min	26.2	27.7	27.6	35.4	37.8
Mean	43.1	45.6	36.1	44.2	46.4
Max	79.4	82.5	55.1	62.6	65.1
St.Dev.	12.3	12.8	7.7	7.2	7.5

n= number of temperatures

Per community, after applying the paleoclimate correction, the most reliable estimate of the geothermal gradient under Ft. Providence was determined from DST temperatures and is 55.7± 12.3 °C km^{-1}. Despite the fact that the number of BHTs and DST temperatures was the same, only one of the four BHT data points is deep enough to be corrected, and resulted in a lower geothermal gradient of 54.8± 6.4 °C km^{-1}. In Kakisa, twice as many BHTs are available than DSTs; these corrected BHTs provide the most reliable estimate of the geothermal gradient of 45.2 ± 6.6 °C km^{-1}. Hay River showed the highest mean geothermal gradient of 59.1 ± 14.9 °C km^{-1} calculated from DST temperatures only. In Enterprise, the most reliable estimate for the geothermal gradient of 44.1 ± 10.6 °C km^{-1} was obtained from the corrected DST temperatures. Despite the fact that the corrected BHTs gave higher values, it is noted that only two BHTs out of the three could be corrected for drilling disturbances due to their shallow depth and the shallow non-corrected temperatures are kept for paleoclimate correction (Table 6 and Figure 9).

Table 6. Geothermal gradient g (°C km^{-1}) in each community.

Preprints.org (www.preprints.org) | NOT PEER-REVIEWED | Posted: 9 May 2024 doi:10.20944/preprints202405.0565.v1

		DST (n=4)	Paleoclimate T_i=-5°C	BHT (n=5)	Forster (b)	Paleoclimate T_i=-5°C
Fort-Providence	Min	40.6	43.3	42.3	42.3	45.2
	Mean	52.6	**55.7**	50.4	51.9	54.8
	Max	71.3	74.8	58.1	58.1	61.0
	St.Dev	12.2	12.3	6.0	6.4	6.4
		DST (n=7)	**Paleoclimate T_i=-5°C**	**BHT (n=14)**	**Khele**	**Paleoclimate T_i=-5°C**
Kakisa	Min	33.0	35.6	27.6	34.8	37.0
	Mean	39.9	42.6	35.8	42.8	**45.2**
	Max	60.9	35.6	52.9	59.9	62.4
	St.De	6.9	7.0	6.6	6.5	6.6
		DST (n=5)	**Paleoclimate T_i=-5°C**	**BHT (n=0)**		
Hay River	Min	41.9	44.8			
	Mean	55.9	**59.1**			
	Max	79.4	82.5			
	St.Dev	14.9	14.9			
		DST (n=4)	**Paleoclimate T_i=-5°C**	**BHT (n=3)**	**Harisson**	**Paleoclimate T_i=-5°C**
Enterprise	Min	33.8	36.2	35.5	29.4	32.8
	Mean	41.5	**44.1**	47.4	42.3	45.7
	Max	56.8	59.8	67.5	67.5	70.8
	St.Dev	10.4	10.6	17.5	21.8	20.8

n= number of temperature measurements. The most reliable estimate of the geothermal gradient is in bold.

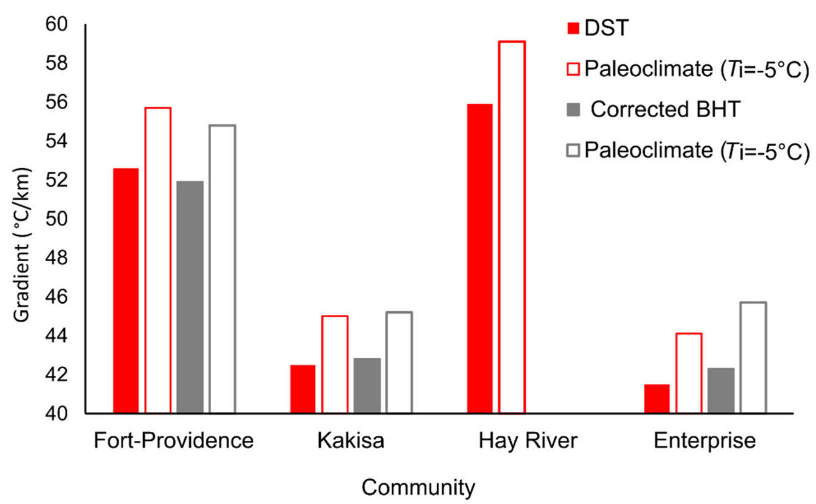

Figure 9. Geothermal gradient estimates of the four South Slave communities.

The average geothermal gradient measured in the six Cameron Hill wells is from 35.4 °C km^{-1} to 43.7 °C km^{-1}, and the paleoclimate correction increases the geothermal gradient from 36.4 °C km^{-1}to 44.6 °C km^{-1} (Table 7).

Table 7. Geothermal gradient g (°C km^{-1}) from Cameron Hills wells.

Well short name	Measured gradient	Gradient paleoclimate

	[°C km^{-1}]	T_i=-5°C [°C km^{-1}]
A-73	39.2	40.2
E-07	43.7	44.6
I-10	35.4	36.4
I-74	42.5	43.5
L-44	37.8	38.8
M-49	43.5	45.3

5.4. Verification with Temperature Profiles from Cameron Hills

5.4.1. Heat flow evaluation for Cameron Hills

Table 8 shows the evaluation of the heat flow considering the thermal conductivity from Table 3. The heat flow is from 80.6 mW m^{-2} to 115.8 mW m^{-2} and the paleoclimate correction increased it to 83.0 mW m^{-2} to 120.6 mW m^{-2}.

Table 8. Surface heat flow from Cameron Hills wells.

Well short name	*Qo* [mW m^{-2}]	*Qo* paleoclimate T_i=-5°C [mW m^{-2}]
A-73	104.1	106.8
E07	113.8	116.0
I-10	80.6	83.0
I-74	105.7	108.3
L-44	102.5	105.1
M-49	115.8	120.6

5.4.2. Temperature-Depth Model

Calculated temperature is compared to measured temperature in the Cameron Hills (Figure 10). The maximum difference is 3.6 °C. Thermal conductivity assigned to the Cameron Hills formations seems logical and allows reproducing observed temperatures.

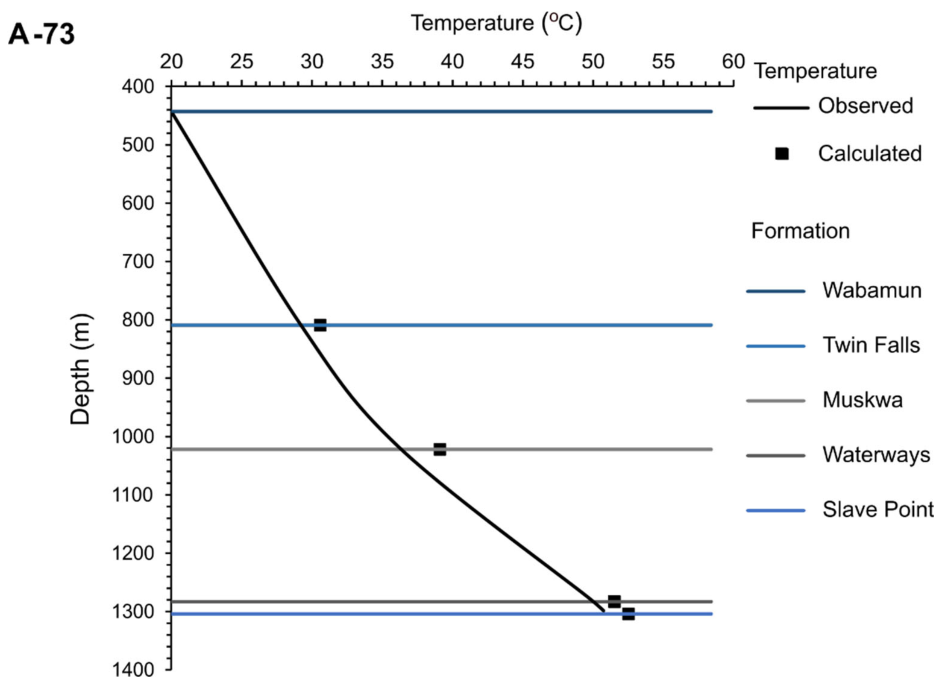

 doi:10.20944/preprints202405.0565.v1

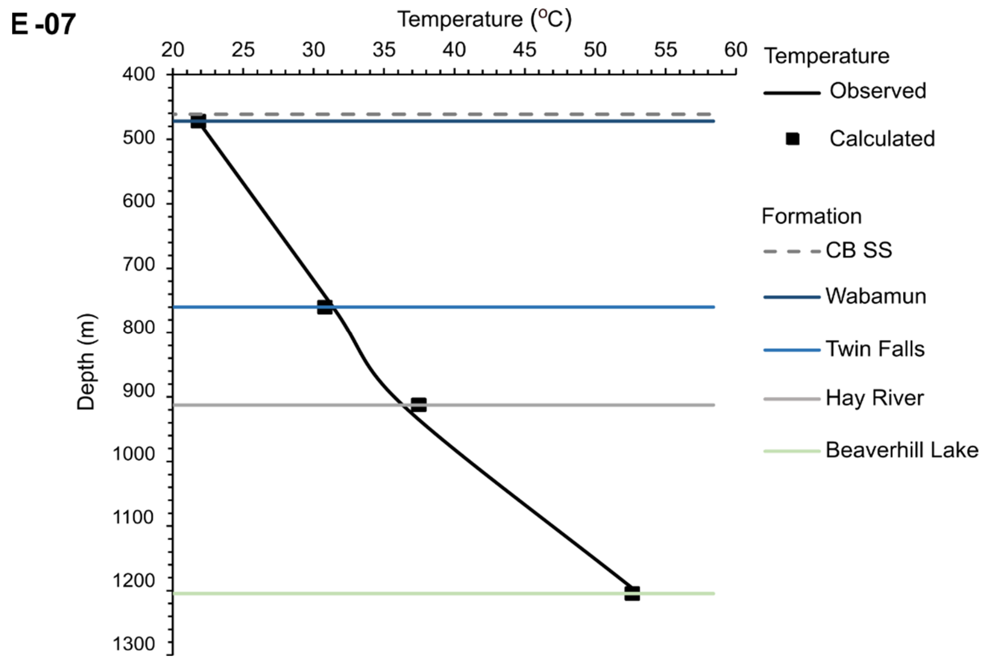

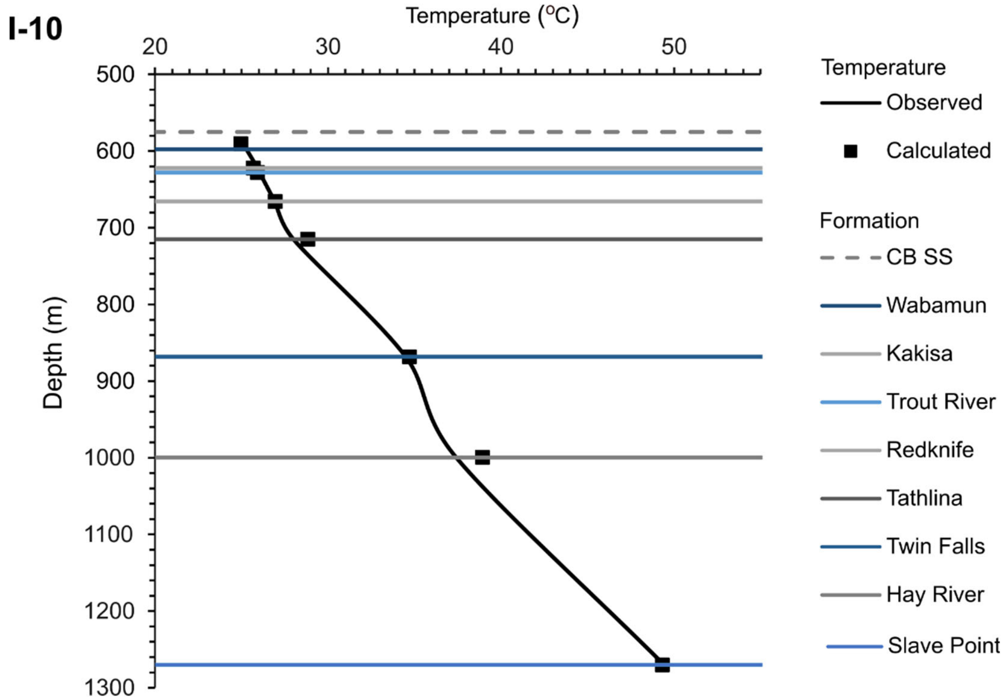

 doi:10.20944/preprints202405.0565.v1

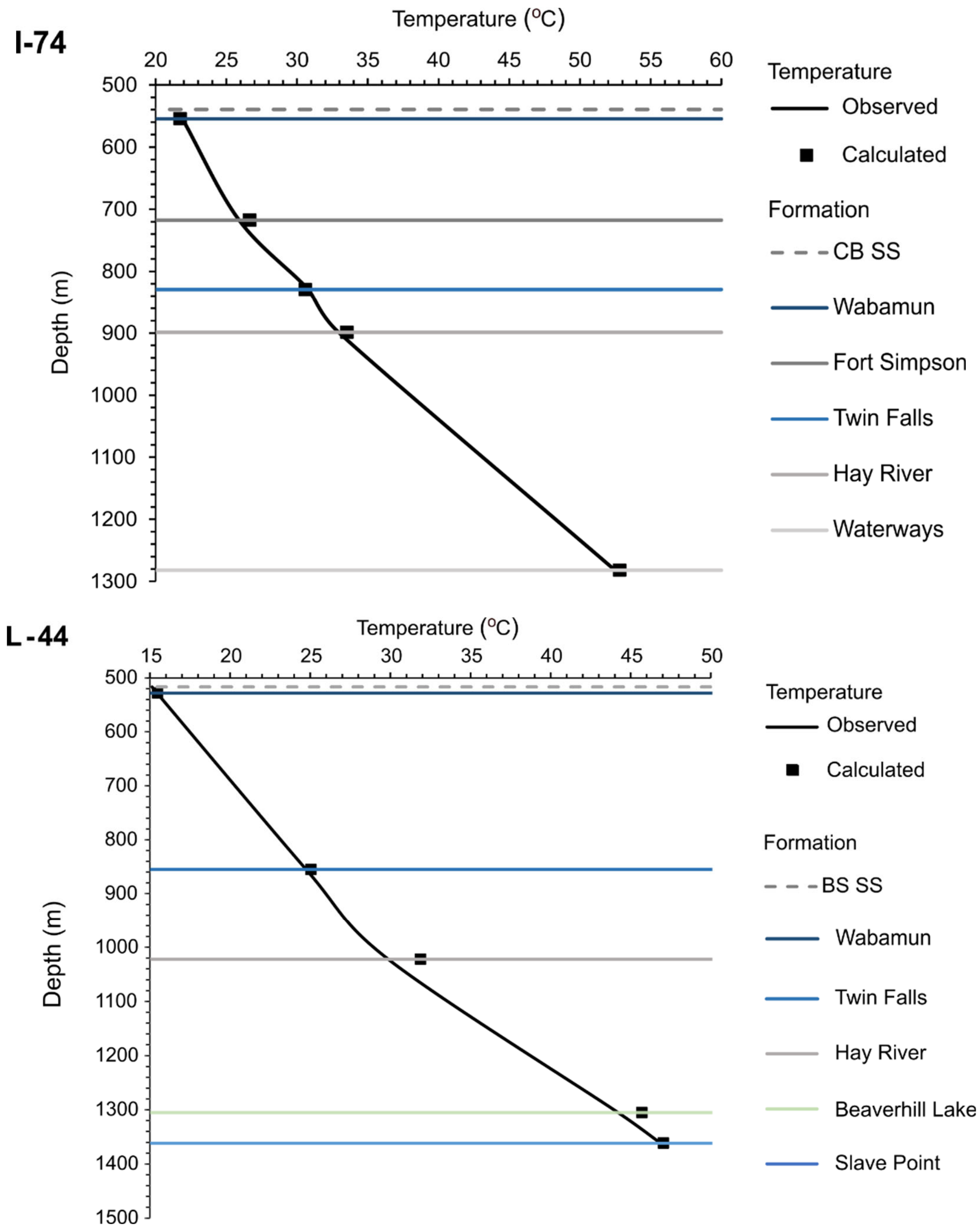

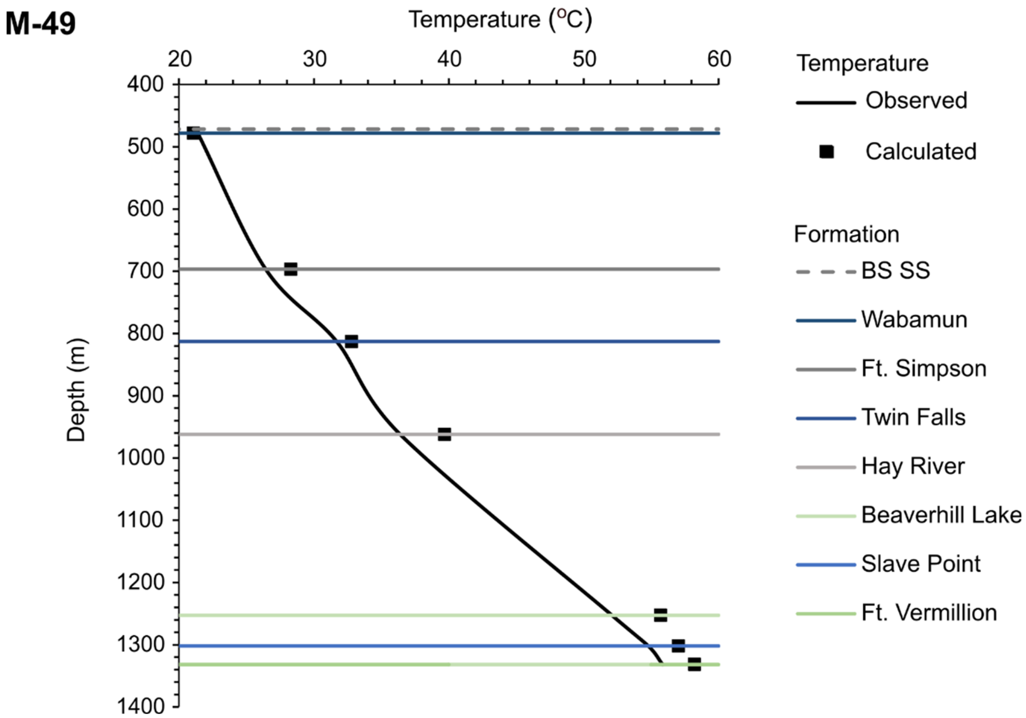

Figure 10. Calculated temperature plotted against observed temperature recorded in the six wells of Cameron Hills region.

5.5. Prediction of Temperature Profiles for South Slave Communities

5.5.1. Heat Flow Evaluation for South Slave Communities

At the community level, the most logical estimation of the heat flow was determined from the most reliable estimate of the geothermal gradient presented in section 4.3 (Table 5). Heat flow assessments are either based on DST or BHT corrected for drilling disturbances, and both temperature data were corrected for paleoclimate effects. The estimate of the surface heat flow in Ft. Providence is 131.5 mW m^{-2}, 105.5 mW m^{-2} in Kakisa, 160.2 mW m^{-2} in Hay River, and 109.3 mW m^{-2} in Enterprise (Figure 11).

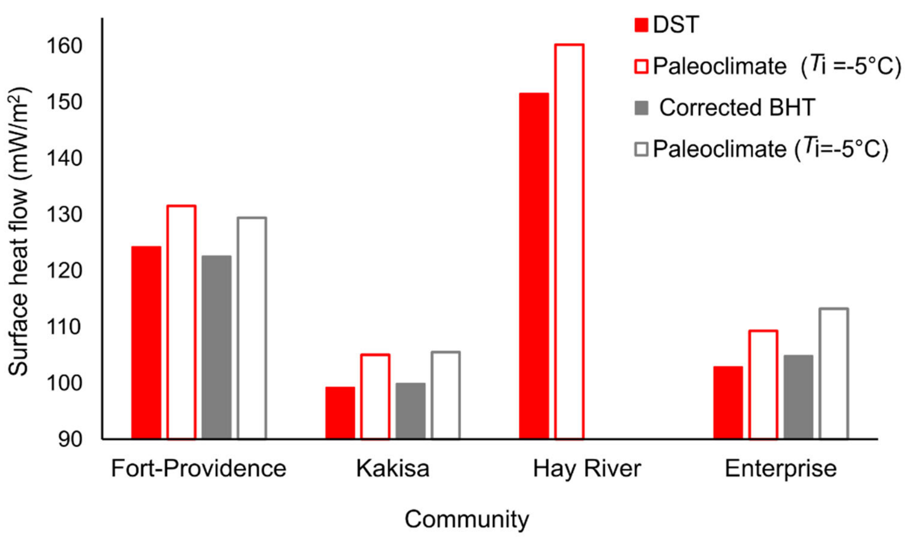

Figure 11. Heat flow estimated for communities of the South Salve Region.

5.5.2. Temperature Depth Model

For all communities, the temperature varies from ~3.2 °C under the Quaternary cover to 33.3 °C at the basement top, with the maximum of 36.5°C in Hay River where the basement top is at 614 m depth. Temperature profiles for Fort Providence, Kakisa, and Enterprise are similar to each other due to the thick shale formations underlying the communities. The maximum temperature reached for these communities is 33.1 °C at the top of the crystalline basement (Figure 12).

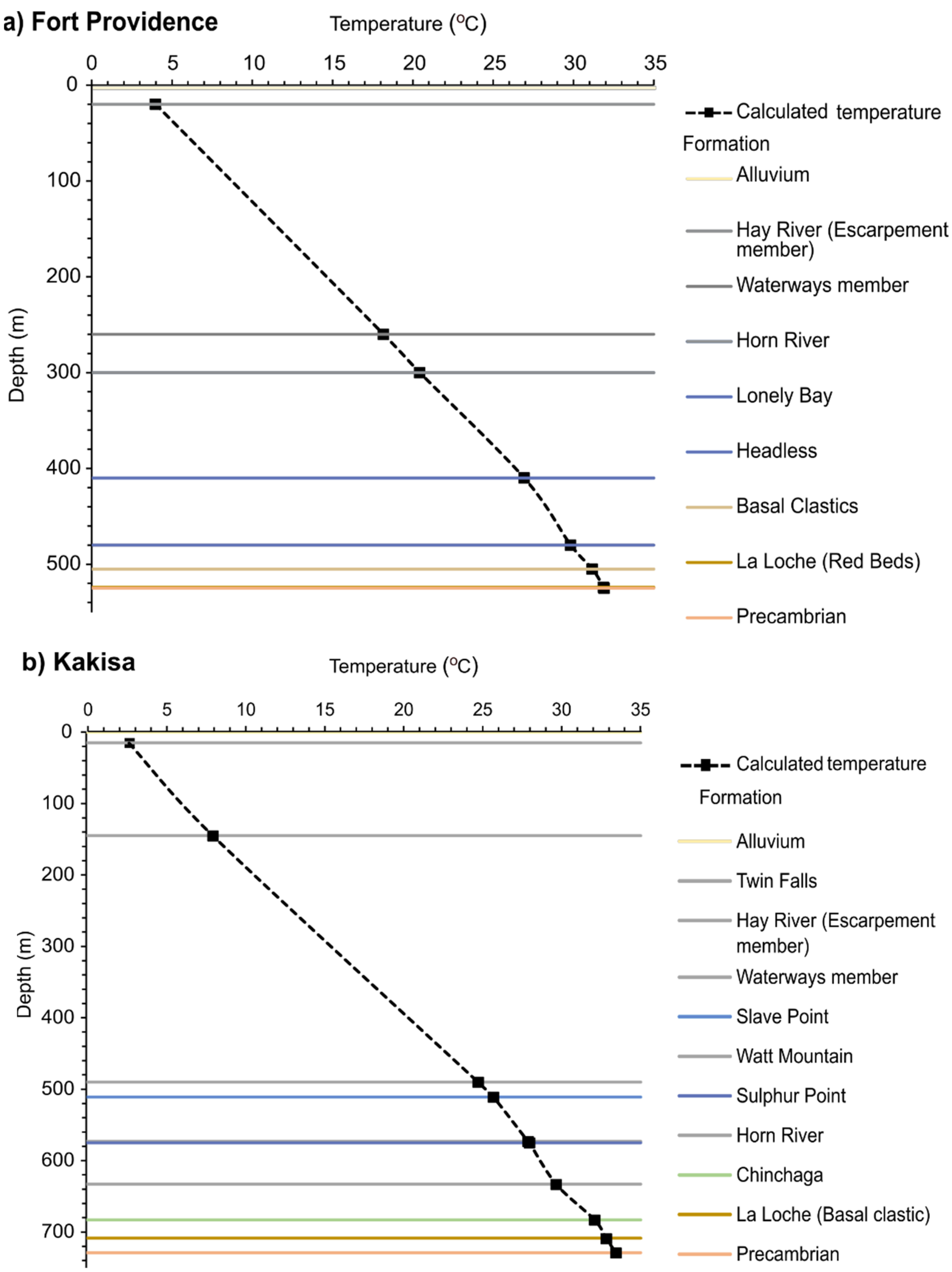

 doi:10.20944/preprints202405.0565.v1

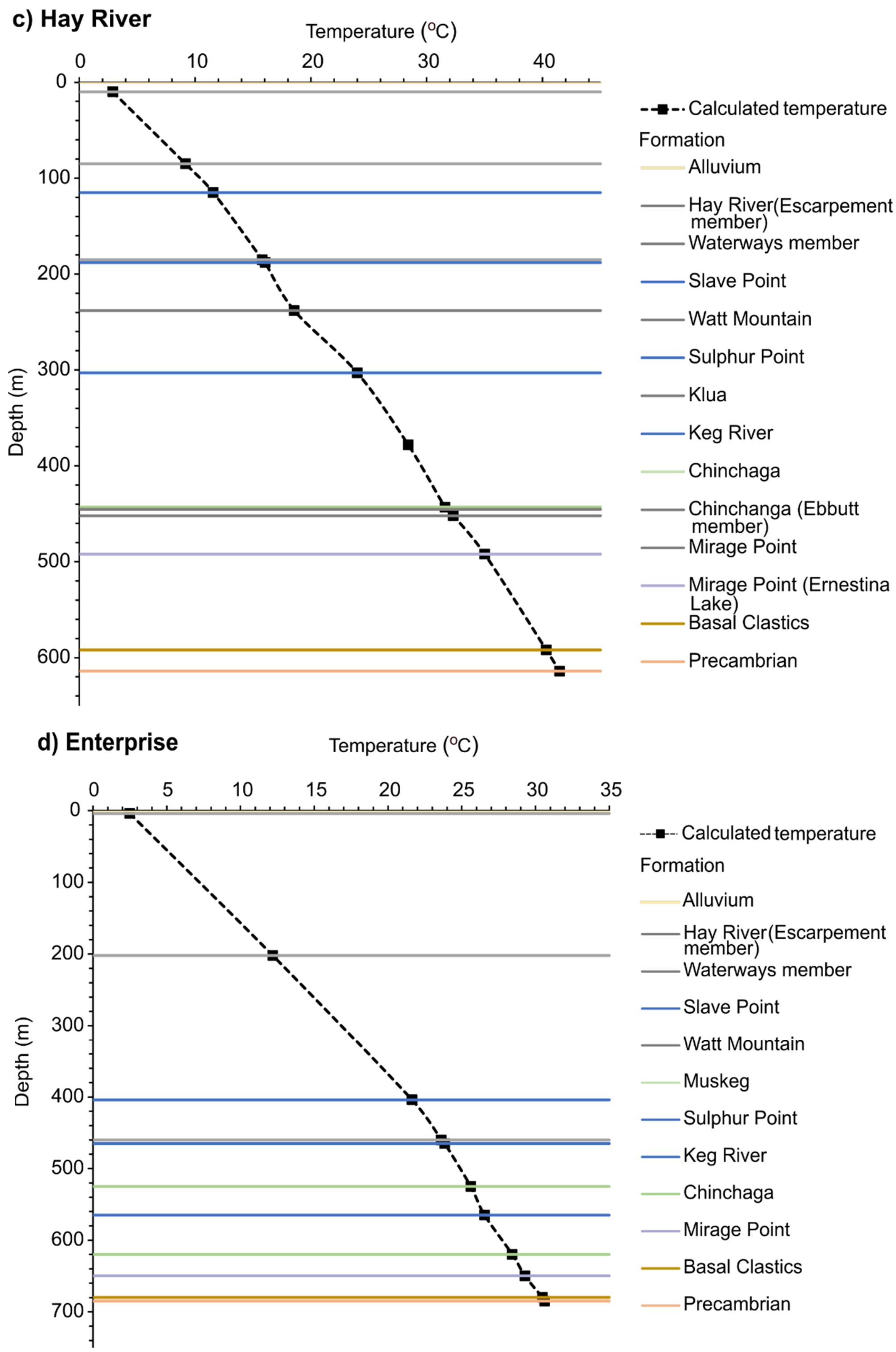

Figure 12. Predicted temperature profiles superposed to the formation tops below each South Slave community.

6. Discussion

Analyses of BHT and DST data (75 readings) from the South Slave Region yielded a local geothermal gradient varying from 45.2 ± 6.6 °C km^{-1} to 59.1 ± 14.9 °C km^{-1} below the communities of Ft. Providence, Kakisa, Hay River, and Enterprise. Heat flow estimates varies from 105.7 mW m^{-2} to 160.2 mW m^{-2} under these communities. These values are comparable to heat flow calculated in the

Preprints.org (www.preprints.org) | NOT PEER-REVIEWED | Posted: 9 May 2024 doi:10.20944/preprints202405.0565.v1

Cameron Hills region where equilibrium temperature profiles were used for verification (Table 8 and Figure 11). The regional temperature distribution throughout the WCSB was previously mapped by other researchers [65,66]. High geothermal gradients (>35 °C km^{-1}) were estimated in the NWT North of 65° latitude with values of 40 °C km^{-1} to 50 °C km^{-1} East of the Mackenzie Mountains [5]. Our work suggest elevated geothermal gradients and heat flows under four communities in the Southern NWT, and confirmed the previous elevated geothermal gradient estimates. These results indicate significant geothermal potential in the communities of Ft. Providence and Hay River. The geothermal gradient in Kakisa and Enterprise is expected > 40 °C km^{-1}, which is again highly favourable, but the small population of those communities could be a challenge for economic exploitation of the geothermal resource.

For this study, no information on the quality of the temperature readings was available, since this relates to the flow rate during the DST and to the mud circulation times for BHT measurements [5]. Limited temperature data was available for each community as they are located in a remote Northern region. The number of temperature data points available in each community was the criterion to determine the most reliable type of data to estimate the geothermal gradient from the group of wells near each community. A large number of BHTs were favoured when possible, but the number of DST temperature was more important for three communities (Ft. Providence, Hay River, and Enterprise).

Measured temperatures from six wells in Cameron Hills was used to verify our thermostratigraphic approach for temperature predictions. A similar approach that uses equilibrium temperature was done for several basins in the USA [23,24]. Majorowicz et al. [67] concluded that even corrected BHTs tend to be systematically higher compared to equilibrium temperature measurements of shallow basins (from 500 to 900 m depth) from wells in the Rocky Mountain Foothills and at the Western edge of the WCSB, and that shallow BHTs contain systematic errors. This was also confirmed and discussed by the works of Majorowicz et al. [68] who estimated the geothermal gradient and regionally mapped the geothermal anomalies of the WCSB. The discrepancies between calculated and observed temperature can be explained by many factors, but the input temperature remains the parameter that has the highest impact on the final geothermal gradient and heat flow estimation [4]. It should also be noted that only Kakisa and Enterprise have temperature data recorded at depth greater than 1km (Figure 7), resulting in the two communities having the lowest gradient, but one that is very similar to the values of Cameron Hills. It is therefore possible that considering data from a shallow depth, like Hay River, resulted in overestimating the geothermal gradient.

Our analyses have demonstrated that the temperature predicted below the four communities present similar trends to that measured for Cameron Hills. The range of thermal conductivity is a source of uncertainty, but verification with temperature profiles in Cameron Hills resulted in small differences of 3.61 °C between calculated and measured temperatures (Figure 10). The radiogenic heat production had a relatively minor impact for the calculation made in this study, since the total thickness of the sedimentary rock formations is less than 1 km. The heat production rate calculated from either radiogenic element content (determined with inductively coupled plasma techniques) or gamma ray is similar for the geological formations common to the South Slave communities (Table 2) and the Cameron Hills (Table 3).

The thermal conductivity is assumed to be uniform in each geological formation, and is responsible for changes in geothermal gradient at geological formation contacts. Lithologies with a lower thermal conductivity shows a relatively more rapid increase in temperature with depth (Figure 12). The most prominent lithologies below the South Slave communities are shales and carbonates. Their estimated thermal conductivity is consistent with thermal conductivity of the typical sedimentary rocks in the WCBS, and have values from 1.4 ± 0.4 W $m^{-1}K^{-1}$ to 2.1 ± 0.4 W $m^{-1}K^{-1}$ in shale, 2.4 ± 0.9 W $m^{-1}K^{-1}$ to 3.4 ± 3.0 $Wm^{-1}K^{-1}$ in limestone, 3.1 ± 1.4 W $m^{-1}K^{-1}$ to 5.0 ± 0.6 $Wm^{-1}K^{-1}$ in dolomite and 2.8 W $m^{-1}K^{-1}$ to 4.7 ± 2.8 W $m^{-1}K^{-1}$ in sandstone [1,69]. The low harmonic average of thermal conductivity estimated for sedimentary rocks below the four communities (~2.5 W $m^{-1}K^{-1}$) reveal its blanketing effect and can partially explain the high geothermal gradient given by the significant thickness of shales in this high heat flow region (Figure 4, Figure 12).

Work described in this manuscript allowed improving the geothermal knowledge of the South Slave Region by using recently acquired information on thermal properties to evaluate heat flow and interpolate subsurface temperature from the surface to the top of the crystalline basement. The regional and deep basement faults that cross the communities (Figure 2) could have an influence on the permeability and convective heat transfer. However, an analysis of the structural context was not addressed in the study area. Natural hydrothermal systems are commonly present in fractured rocks, and typically associated with extensional faulting [70–72]. This is a limitation of our study that focused on conductive heat transfer mechanisms only.

7. Conclusions

Compilation of DST temperature and BHT that were corrected for drilling disturbances allowed evaluation of the geothermal gradient and heat flow below communities of the South Slave Region to subsequently predict the temperature-depth distribution in the sedimentary basin formations. The current estimation of the geothermal gradient is > 40 °C km^{-1} and up to 100 mW m^{-2} for heat flow.

The result indicates high geothermal gradient and high surface heat flow suitable for direct use of geothermal resources at the depth of sedimentary rock formations according to the Lindal diagram [73]. The communities, particularly Hay River, could potentially exploit the geothermal resource. Here, the high geothermal gradient could facilitate exploitation at shallow drilling depth and result in potentially economic projects.

The heat flow in the South Slave Region would be the highest of all the WCSB according to this modeling work, but geothermal exploration boreholes will have to be drilled to confirm these results. Drilling exploration wells and measuring equilibrium temperature profiles are the next steps to confirm our finding and eventually exploit geothermal resources. The use of thermally equilibrated temperature measurement data from wells in the Cameron Hills allowed verification of our model to determined if the thermal conductivities assigned to the geological formations underlying the South Slave communities is logical, using formations common to both areas (Twin Falls, Hay River, and Slave Point Formations). The thermal conductivity values of the sedimentary rocks varies from 1.4 W m^{-1} K^{-1} to 3.5 W m^{-1} K^{-1}. However, the nature and the thermal properties of the Precambrian basement below the sedimentary basin at the location of the South Slave communities need to be defined in future work in order to extrapolate the temperature at depth below the basin. Evaluating the thermal conductivity of the crystalline basement will be crucial to get a reliable estimate of temperature in deep basement rocks

Supplementary data: The following supporting information can be downloaded at the website of this paper posted on Preprints.org., DST and uncorrected BHT are presented as a Supplementary data.

Author Contributions: Conceptualization, M.R. and J.R.; methodology, M.R and J.R.; validation, J.R., F-A.C.,M.T.,E.J.S, and V.T.; formal analysis, M.R.; investigation, M.R.,M.T.; resources, J.R.,V.T.; writing—original draft preparation, M.R.; writing—review and editing, J.R., F-A.C., M.T., E.J.S, and V.T.; visualization, M.R.; supervision, J.R.; project administration, J.R.; funding acquisition, J.R. All authors have read and agreed to the published version of the manuscript."

Funding: This project was funded by GEM-GeoNorth program of Natural Resources Canada.

Data Availability: The relevant datasets analyzed in this study are all presented in the manuscript.

Acknowledgements: we would like to thank Hickson C. J., [12] who made available the temperature data of Cameron Hills wells through the collaborative work of geothermal development and energy sustainability decisions in the Dehcho Region.

Conflicts of Interest: The authors declare no conflicts of interest.

References

1. Jessop, A.M. Chapter 3—Analysis and Correction of Heat Flow on Land. In *Developments in Solid Earth Geophysics*, ed.; Jessop, A.M. Eds.; Elsevier: 1990; Volume 17, pp. 57-85.doi:https://doi.org/10.1016/B978-0-444-88309-4.50007-5
2. Majorowicz, J., Šafanda, J., and Torun-1 Working, G. Heat flow variation with depth in Poland: evidence from equilibrium temperature logs in 2.9-km-deep well Torun-1. *International Journal of Earth Sciences* **2008**, *97*, 307-315. doi:10.1007/s00531-007-0210-2
3. Augustine, C., Tester, J.W., Anderson, B., Petty, S., and Livesay, B. A comparison of geothermal with oil and gas well drilling costs. In Proceedings of 31st Workshop on Geothermal Reservoir Engineering, Stanford, California, USA, 30 February.2006
4. Bédard, K., Comeau, F.-A., Raymond, J., Malo, M., and Nasr, M. Geothermal Characterization of the St. Lawrence Lowlands Sedimentary Basin, Québec, Canada. *Natural Resources Research* **2018**, *27*, 479-502. doi:10.1007/s11053-017-9363-2
5. Grasby, S., Majorowicz, J., and McCune, G. Geothermal energy potential for northern communities Open File; 2013. Report No: 7350.
6. Harrison, W.E., Luza, K.V., Prater, M.L., and Reddr, R.J. Geothermal resource assessment in Oklahoma Special paper; 1983. Report No: DE-AS07-80ID12172.
7. Majorowicz, J. and Grasby, S.E. Deep Geothermal Heating Potential for the Communities of the Western Canadian Sedimentary Basin. *Energies* **2021**, *14*, 1-37. doi:https:// doi.org/10.3390/en14030706
8. Grasby, S.E., Allen, D.M., Bell, S., Chen, Z., Ferguson, G., Jessop, A., Kelman, M., Majorowicz, M., Ko, J., Moore, M., Raymond, J., and Therrien, R. Geothermal energy resource potential of Canada Open File (revised); 2011. Report No: 6914.
9. EBA Engineering Consultants Ltd. Geothermal Favourability Map Northwest Territories Report 2010. Report No: Y22101146.
10. Petrel Robertson Consulting Ltd. Geothermal database compilation Internal Report; 2022.
11. OROGO(2022) Well Status files. Office of the Regulator of Oil and Gas Operations.https://www.orogo.gov.nt.ca/en/resources-0. Accessed on January 2022.
12. Smejkal, E.J., Hickson, C.J., and Collard, J. Revisiting the geothermal potential of the Dehcho Region in NWT: New data from old wells. In Proceedings of Geoconvention Calgary, AB Canada, 15-17 May.2023
13. Carvalho, H.D.S. and Vacquier, V.D. Method for determining terrestrial heat flow in oil fields. *Geophysics* **1977**, *42*, 584-593. doi:https://doi.org/10.1190/1.1440729
14. Canadian Sedimentary Basin. *Tectonophysics* **1981**, *74*, 209-238. doi:https://doi.org/10.1016/0040-1951(81)90191-8
15. Reiter, M. and Jessop, A.M. Estimates of terrestrial heat flow in offshore eastern Canada. *Canadian Journal of Earth Sciences* **1985**, *22*, 1503-1517. doi:10.1139/e85-156
16. Kenneth, E.P. and Philip, H.N. Criteria to Determine Borehole Formation Temperatures for Calibration of Basin and Petroleum System Models. In Proceedings of AAPG Annual Convention and Exhibition, Denver, Colorado, USA, June 7-10.2009
17. Deming, D. and Chapman, D.S. Heat Flow in the Utah-Wyoming Thrust Belt From Analysis of Bottom-Hole Temperature Data Measured in Oil and Gas Wells. *Journal of Geophysical Research: Solid Earth* **1988**, *93*, 13657-13672. doi:https://doi.org/10.1029/JB093iB11p13657
18. Dowdle, W.L. and Cobb, W.M. Static Formation Temperature From Well Logs—An Empirical Method. *Journal of Petroleum Technology* **1975**, *27*, 1326-1330. doi:10.2118/5036-pa
19. Förster, A., Merriam, D., and Davis, J. Spatial analysis of temperature (BHT/DST) data and consequences for heat-flow determination in sedimentary basins. *International Journal of Earth Sciences* **1997**, *86*, 252-261. doi:10.1007/s005310050138
20. Blackwell, D.D. and Richards, M. Geothermal Map of North America. AAPG Map, scale Calibration of the AAPG Geothermal Survey of North America BHT data base. In Proceedings of AAPG Annual Meeting, Poster session, paper 87616, Dallas TX, 18-21 April 2004
21. Blackwell, D.D., Richards, M., and Stepp, P. Texas geothermal assessment for the I35 corridor east Final report; 2010. Report No: CM709.
22. Gregory, A., Dodge, M., Posey, J., and Morton, R. Volume and accessibility of entrained (solution) methane in deep geopressured reservoirs-Tertiary formations of the Texas Gulf Coast. DOE Final Report; 1980. Report No: DOE/ET/11397-1.
23. Crowell, A.M., Ochsner, A.T., and Gosnold, W. Correcting Bottom-Hole Temperatures in the Denver Basin: Colorado and Nebraska. In Proceedings of Geothermal Resources Council Annual Meeting 2012, Reno, Nevada, USA, 30 September—3 October.2012
24. Crowell, A. and Gosnold, W. Correcting Bottom Hole Temperatures: A Look at the Permian Basin (Texas), Williston Basin (North Dakota), Anadarko and Arkoma Basins (Oklahoma). In Proceedings of Geothermal Resources Council Annual Meeting 2011, San Diego, CA, USA, 23-26 October.2011

25. Westaway, R. and Younger, P., L. Accounting for palaeoclimate and topography: A rigorous approach to correction of the British geothermal dataset. *Geothermics* **2013**, *48*, 31-51. doi:https://doi.org/10.1016/j.geothermics.2013.03.009
26. Dyke, A.S. An outline of North American deglaciation with emphasis on central and northern Canada. In *Developments in Quaternary Sciences*, ed.; Ehlers, J. and Gibbard, P.L. Eds.; Elsevier: 2004; Volume 2, pp. 373-424.doi:https://doi.org/10.1016/S1571-0866(04)80209-4
27. Lemmen, D.S., Duk-Rodkin, A., and Bednarski, J.M. Late glacial drainage systems along the northwestern margin of the Laurentide Ice Sheet. *Quaternary Science Reviews* **1994**, *13*, 805-828. doi:https://doi.org/10.1016/0277-3791(94)90003-5
28. Gal, L.P. and Jones, A.L. Evaluation of oil and gas potential in the Deh Cho territory Open File; 2003. Report No: 2003-03.
29. Stott, D.F. and Klassen, R.W. Geomorphic divisions. In *Sedimentary Cover of the Craton in Canada*, ed.; Stott, D.F. and Aitken, J.D. Eds.; Geological Survey of Canada, Geology of Canada: 1993; Volume 5, pp. 31-44.
30. Meijer Drees, N.C.*The Devonian succession in the subsurface of the Great Slave and Great Bear plains, Northwest Territories*, ed.; Geological Survey of Canada: Ontario, Canada, 1993; p. 231.doi:https://doi.org/10.4095/183905
31. Moore, P.F. Devonian. In *Sedimentary Cover of the Craton in Canada*, ed.; Stott, D.F. and Aitken, J.D. Eds.; Geological Survey of Canada, Geology of Canada: 1993; Volume 5, pp. 150-201.
32. Morrow, D.W. and Geldsetzer, H.H.J. Devonian of the eastern Canadian Cordillera. In *Devonian of the World Regional syntheses* ed.; N.J. McMillan, Embry, A.F., and Glass, D.J. Eds.; Canadian Society of Petroleum Geologists: 1988; Volume 1, pp. 85-121.
33. Mossop, G. and Shetsen, I. (1994). Geological Atlas of the Western Canada Sedimentary Basin. https://ags.aer.ca/reports/atlas-western-canada-sedimentary-basin. accessed on 12 January. 2022
34. Wright, G., McMechan, M., and Potter, D. Structure and architecture of the Western Canada sedimentary basin. In *Geological atlas of the Western Canada sedimentary basin*, ed.; Mossop, G. and Dixon, J. Eds.; Canadian Society of Petroleum Geologists and Alberta Research Council: 1994; Volume 4, pp. 25-40.
35. Smith, I.R., Christine, D., Grant, H., and Roger, C.P. A drift isopach model for the southwestern Great Slave Lake region, Northwest Territories, Canada. *Journal of Maps* **2022**, 1-12. doi:https://doi.org/10.1080/17445647.2022.2147871
36. Morrow, D.W., MacLean, B.C., Tzeng, P., and Pana, D. Subsurface Paleozoic structure and isopach maps and selected seismic lines in southern Northwest Territories and northern Alberta: implications for mineral and petroleum potential Open File; 2002. Report No: 4366.
37. Rocheleau, J. and Fiess, K.M. Northwest Territories Oil and Gas Poster Series: Basins & Petroleum Resources, Table of Formations, Schematic Cross Sections Open File; 2014. Report No: 2014-03.
38. Northwest Territories Geological Survey(2023) Geology Map. https://ntgs-open-data-ntgs.hub.arcgis.com/. Accessed on 2nd august 2022.
39. Ouzzane, M., Eslami-nejad, P., Badache, M., and Aidoun, Z. New correlations for the prediction of the undisturbed ground temperature. *Geothermics* **2015**, *53*, 379-384. doi:https://doi.org/10.1016/j.geothermics.2014.08.001
40. Environment and Climate Change Canada(2019) Historical Climate Data. Canada: Government of Canada. http://climate.weather.gc.ca/. Accessed on 20 April 2023.
41. Rajaobelison., M., Thibault., M., Comeau., F.-A., Raymond., J., and Terlaky., V. Laboratory analyses on split core samples from wells to assess the geothermal potential of the South Slave Region, Northwest Territories, Canada Open Report; in press. Report No: OR 2023-015.
42. Beardsmore, G. and Cull, J.*Crustal heat flow: a guide to measurement and modelling*, 1st ed.; Cambridge University Press: New York, USA, 2001; p. 324.doi:https://doi.org/10.1046/j.1365-246X.2003.01914.x
43. Jaupart, C. and Mareschal, J.-C.*Heat generation and transport in the Earth*, ed.; Cambridge university press: New York, USA, 2010; p. 462.
44. Popov, Y.A., Beardsmore, G., Clauser, C., and Roy, S. ISRM suggested methods for determining thermal properties of rocks from laboratory tests at atmospheric pressure. *Rock Mechanics and Rock Engineering* **2016**, *49*, 4179-4207. doi:10.1007/s00603-016-1070-5
45. Clauser, C. and Huenges, E. Thermal conductivity of rocks and minerals. In *Rock Physics and Phase Relations*, ed.; Ahrens, T.J. Eds.; AGU Reference Shelf 3: 1995; Volume pp. 105-126.doi:https://doi.org/10.1029/RF003p0105
46. Eppelbaum, L., Kutasov, i., and Pilchin, A.*Applied Geothermics*, ed.; Springer Heidelberg New York Dordrecht London, 2014; p. 757.doi:https://doi.org/10.1007/978-3-642-34023-9
47. Larmagnat, S., Lavoie, D., Rajaobelison, M.M., and Raymond, J. Geothermal assessment of a conventional hydrocarbon reservoir in eastern Québec: preliminary field and petrophysical data Open File; 2019. Report No: 8597.

48. Mielke, P., Bär, K., and Sass, I. Determining the relationship of thermal conductivity and compressional wave velocity of common rock types as a basis for reservoir characterization. *Journal of Applied Geophysics* **2017**, *140*, 135-144. doi:https://doi.org/10.1016/j.jappgeo.2017.04.002
49. Tang, B., Zhu, C., Xu, M., Chen, T., and Hu, S. Thermal conductivity of sedimentary rocks in the Sichuan basin, Southwest China. *Energy Exploration & Exploitation* **2018**, *37*, 691-720. doi:https://doi.org/10.1177/0144598718804902
50. Cermak, V. and Rybach, L. Thermal Conductivity and Specific Heat of Minerals and Rocks. In *Physical Properties of Rocks · SubVolume A*, ed.; Angenheister, G. Eds.; Springer: Berlin, Heidelberg and New York,1982; Volume 1A, pp. 305–343.doi:10.1007/10201894_62
51. Pasquale, V., Verdoya, M., and Chiozzi, P. Measurements of rock thermal conductivity with a Transient Divided Bar. *Geothermics* **2015**, *53*, 183-189. doi:https://doi.org/10.1016/j.geothermics.2014.05.008
52. Bücker, C. and Rybach, L. A simple method to determine heat production from gamma-ray logs. *Marine and Petroleum Geology* **1996**, *13*, 373-375. doi:https://doi.org/10.1016/0264-8172(95)00089-5
53. Hasterok, D., Gard, M., and Webb, J. On the radiogenic heat production of metamorphic, igneous, and sedimentary rocks. *Geoscience Frontiers* **2018**, *9*, 1777-1794. doi:https://doi.org/10.1016/j.gsf.2017.10.012
54. Waples, D.W. A New Model for Heat Flow in Extensional Basins: Estimating Radiogenic Heat Production. *Natural Resources Research* **2002**, *11*, 125-133. doi:10.1023/A:1015568119996
55. Burrus, J. and Foucher, J.P. Contribution to the thermal regime of the Provençal Basin based on Flumed heat flow surveys and previous investigations. *Tectonophysics* **1986**, *128*, 303-334. doi:https://doi.org/10.1016/0040-1951(86)90299-4
56. Kehle, R.O., Schoeppel, R.J., and Deford, R.K. The AAPG geothermal survey of North America. *Geothermics* **1970**, *2*, 358-367. doi:https://doi.org/10.1016/0375-6505(70)90034-9
57. Richards, M.Crowell, A.M. SMU Geothermal Laboratory.Personal Communication, 2012
58. Mareschal, J.C. and Jaupart, C. Variations of surface heat flow and lithospheric thermal structure beneath the North American craton. *Earth and Planetary Science Letters* **2004**, *223*, 65-77. doi:https://doi.org/10.1016/j.epsl.2004.04.002
59. Majorowicz, J., Gosnold, W., Gray, A., Safanda, J., Klenner, R., and Unsworth, M. Implications of post-glacial warming for northern Alberta heat flow-correcting for the underestimate of the geothermal potential. In Proceedings of Geothermal Resources Council Annual Meeting 2012 Reno, Nevada, USA, 30 September—3 October.2012
60. Beltrami, H., Gosselin, C., and Mareschal, j.-c. Ground surface temperatures in Canada: Spatial and temporal variability. *Geophysical Research Letters* **2003**, *30*, 6-1. doi:10.1029/2003GL017144
61. Birch, A.F. The effects of Pleistocene climatic variations upon geothermal gradients. *American Journal of Science* **1948**, *246*, 729. doi:10.2475/ajs.246.12.729
62. Jessop, A.M. The Distribution of Glacial Perturbation of Heat Flow in Canada. *Canadian Journal of Earth Sciences* **1971**, *8*, 162-166. doi:10.1139/e71-012
63. Stein, C.A. Heat Flow of the Earth. In *Global Earth Physics*, ed.; Eds.; 1995; Volume pp. 144-158.doi:https://doi.org/10.1029/RF001p0144
64. Turcotte, D.L. and Schubert, G.*Geodynamics*, 3rd ed.; Cambridge University Press: New York, USA, 2014; p. 615.doi:
65. Majorowicz, J. and Grasby, S.E. Heat flow, depth–temperature variations and stored thermal energy for enhanced geothermal systems in Canada. *Journal of Geophysics and Engineering* **2010**, *7*, 232-241. doi:10.1088/1742-2132/7/3/002
66. Allan Gray, D., Majorowicz, J., and Unsworth, M. Investigation of the geothermal state of sedimentary basins using oil industry thermal data: case study from Northern Alberta exhibiting the need to systematically remove biased data. *Journal of Geophysics and Engineering* **2012**, *9*, 534-548. doi:10.1088/1742-2132/9/5/534
67. Majorowicz, J.A., Garven, G., Jessop, A., and Jessop, C. Present Heat Flow Along a Profile Across the Western Canada Sedimentary Basin: The Extent of Hydrodynamic Influence. In *Geothermics in Basin Analysis*, ed.; Förster, A. and Merriam, D.F. Eds.; Springer US: Boston, MA USA,1999; Volume pp. 61-79.doi:10.1007/978-1-4615-4751-8_3
68. Majorowicz, A.G., D,Jacek, and Unsworth, M. Investigation of the geothermal state of sedimentary basins using oil industry thermal data: case study from Northern Alberta exhibiting the need to systematically remove biased data. *Journal of Geophysics and Engineering* **2012**, *9*, 534-548. doi:10.1088/1742-2132/9/5/534
69. Beach, R.D.W., Jones, F.W., and Majorowicz, J.A. Heat flow and heat generation estimates for the churchill basement of the western canadian basin in Alberta, Canada. *Geothermics* **1987**, *16*, 1-16. doi:https://doi.org/10.1016/0375-6505(87)90075-7
70. Faulds, J., Coolbaugh, M., Bouchot, V., Moeck, I., and Oguz, K. Characterizing structural controls of geothermal reservoirs in the Great Basin, USA, and Western Turkey: Developing successful exploration strategies in extended terranes. In Proceedings of World Geothermal Congress Bali, 25-30 April.2010

71. Moeck, I. A new classification scheme for deep geothermal systems based on geologic controls. In Proceedings of EGU General Assembly Conference Abstracts, Vienna, Austria, 22–27 April.2012
72. Rajaobelison, M., Raymond, J., Malo, M., Dezayes, C., and Larmagnat, S. Understanding heat transfer along extensional faults: The case of the Ambilobe and Ambanja geothermal systems of Madagascar. *Geothermics* **2022**, *104*, 102455. doi:https://doi.org/10.1016/j.geothermics.2022.102455
73. Lindal, B. Industrial and other applications of geothermal energy. *Geothermal energy* **1973**, 135-148.